Comparison of $S=0$ and $S=\frac{1}{2}$ impurities in the Haldane chain compound Y$_2$BaNiO$_5$

J. Das,[1] A. V. Mahajan,[1] J. Bobroff,[2] H. Alloul,[2] F. Alet,[3,4] and E. S. Sørensen[5]

[1]*Department of Physics, Indian Institute of Technology, Mumbai 400076, India*
[2]*Laboratoire de Physique des Solides, UMR 8502, Université Paris-Sud, 91405 Orsay, France*
[3]*Theoretische Physik, ETH Zürich, CH-8093 Zürich, Switzerland*
[4]*Computational Laboratory, ETH Zürich, CH-8092 Zürich, Switzerland*
[5]*Department of Physics and Astronomy, McMaster University, Hamilton, Ontario, L8S 4M1 Canada*

We present the effect of Zn ($S=0$) and Cu ($S=1/2$) substitution at the Ni site of $S=1$ Haldane chain compound Y$_2$BaNiO$_5$. ^{89}Y nuclear-magnetic resonance (NMR) allows us to measure the local magnetic susceptibility at different distances from the defects. The ^{89}Y NMR spectrum consists of one central peak and several less intense satellite peaks. The central peak represents the chain sites far from the defect. Its shift measures the uniform susceptibility, which displays a Haldane gap $\Delta \approx 100$ K and it corresponds to an antiferromagnetic (AF) coupling $J \approx 260$ K between the nearest neighbor Ni spins. Zn or Cu substitution does not affect the Haldane gap. The satellites, which are evenly distributed on the two sides of the central peak, probe the antiferromagnetic staggered magnetization near the substituted site. The spatial variation of the induced magnetization is found to decay exponentially from the impurity for both Zn and Cu for $T>50$ K. Its extension is found identical for both impurities and corresponds accurately to the correlation length $\xi(T)$ determined by Monte Carlo simulations for the pure compound. In the case of nonmagnetic Zn, the temperature dependence of the induced magnetization is consistent with a Curie law with an "effective" spin $S=0.4$ on each side of Zn. This staggered effect is quantitatively well accounted for in all the explored range by quantum Monte Carlo (QMC) computations of the spinless-defect-induced magnetism. In the case of magnetic Cu, the similarity of the induced magnetism to the Zn case implies a weak coupling of the Cu spin to the nearest-neighbor Ni spins. The slight reduction of about $20-30\%$ of the induced polarization with respect to Zn is reproduced by QMC computations by considering an antiferromagnetic coupling of strength $J'=0.1J-0.2J$ between the $S=1/2$ Cu spin and nearest-neighbor Ni spin. Macroscopic susceptibility measurements confirm these results as they display a clear Curie contribution due to the impurities nearly proportional to their concentration. This contribution is indeed close to that of two spin half for Zn substitution. The Curie contribution is smaller in the Cu case, which confirms that the coupling between Cu and near-neighbor Ni is antiferromagnetic.

PACS number(s): 75.30.Hx, 75.40.Cx, 76.60.Cq

I. INTRODUCTION

One- and two-dimensional Heisenberg antiferromagnetic (1D and 2D HAF) spin systems are presently attracting strong interest due to the variety of ground states that these systems exhibit: spin gap, spin Peierls, resonating valence bond, superconductivity, etc. Effects of substitution in the HAF half-integer[1] and integer-spin chains,[2] ladders,[3] and planes[4] have been studied both experimentally and theoretically to understand such ground states and their elementary excitations.

Among these systems, one-dimensional $S=1$ HAF chains have attracted immense interest after Haldane[5] conjectured that in case of integer-spin chains, there is a finite energy gap between the ground state and first excited state. The ground state of this system can be well described by valence bond solid (VBS) model.[6] This model suggests that each $S=1$ spin can be considered to be a symmetric combination of two $S=1/2$ spins. With periodic boundary conditions, each $S=1/2$ forms a singlet with the nearest neighbor (nn) belonging to the adjacent site. Introducing a nonmagnetic impurity, i.e., open boundary conditions, is equivalent to removing one $S=1$. This is expected to give rise to two $S=1/2$ at each end of the chain.[7]

Y$_2$BaNiO$_5$ (YBNO), an $S=1$ one-dimensional HAF is a well-established Haldane gap compound. YBNO can be described by the space group I_{mmm}.[8] All the Ni^{2+} ions are located at the center of highly compressed corner shared NiO$_6$ octahedra and form Ni-O-Ni chains along the a axis [see Fig. 1(a)]. These octahedra are flattened along the chain axis and the Ni-O distances can be divided in two groups (Ni-O1 ≈ 1.885 Å and Ni-O2 ≈ 2.186 Å). Intrachain Ni-Ni distance is equal to 3.77 Å (Ni^{2+} ions interact via the oxygen ion), while the smallest interchain Ni-Ni distance is close to 6.6 Å. Also, since these chains are separated by Ba and Y cations, the physical properties are expected to be predominantly 1D. The superexchange coupling J estimated from magnetic susceptibility is $J \approx 285$ K.[9] The magnitude of the Haldane gap $\Delta \approx 100$ K has been obtained from magnetic susceptibility measurements.[9–11] Inelastic neutron-scattering experiments also reveal the existence of a gap $\Delta \approx 100$ K,[9,12] between the ground state and first excited state and $|J_\perp / J| < 5 \times 10^{-4}$, where $J_\perp$ and J are the interchain and intrachain coupling constants, respectively.[13] This proves the strong 1D character of the Ni chains. ^{89}Y nuclear-magnetic-resonance (NMR) experiments on polycrystalline YBNO[14] also show the presence of a gap $\Delta = 80 \pm 5$ K and an anisotropic shift which is responsible for the asymmetry in the NMR spectra.

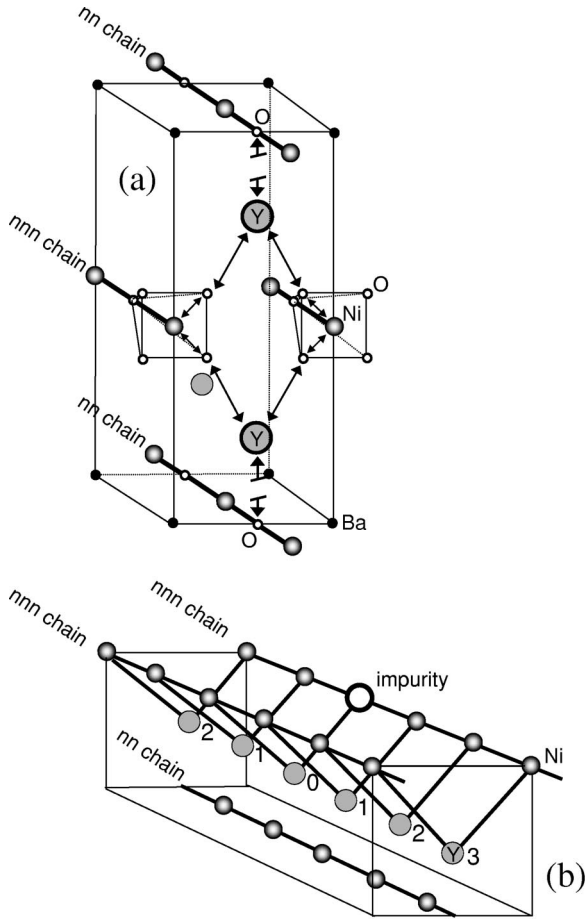In-chain Zn^{2+}, Mg^{2+} ($S=0$) substitutions at the Ni^{2+}

FIG. 1. (a) Representation of the unit cell of Y_2BaNiO_5: the ^{89}Y nucleus is hyperfine coupled to the Ni electrons in its two next-nearest-neighbor (nnn) chains through oxygens while its transferred hyperfine coupling to the Ni on the nearest-neighbor (nn) chain is expected to be small. (b) When an impurity is substituted in one of the two nnn chains, ^{89}Y nuclei which couple to that chain are labeled according to their distance to the impurity as indicated in the figure. In (a) only some of the oxygen atoms are represented, for clarity. In (b) only the Ni and Y sites are displayed.

($S=1$) site of YBNO (Refs. 2 and 15–18) have been attempted. Bulk susceptibility measurements confirm that nonmagnetic substitutions break the chains and give rise to chain-end free spins.[16] Low-temperature specific-heat measurements[15] on different doped samples have been quantitatively explained by an effective model,[19] which describes the low-energy spectrum of noninteracting open $S=1$ chain. Tedoldi *et al.*[17] carried out ^{89}Y NMR experiments in 5% and 10% Mg doped YBNO for temperatures $T>\Delta$. They observed multiple-peak ^{89}Y NMR spectra at different T and determined the T dependence of the staggered magnetization near the impurity from the shift of these peaks at different T. From the site dependence of the staggered magnetization, the characteristic length scale of its decay was found to be similar to the correlation length $\xi(T)$ of the pure $S=1$ HAF chain. At lower temperatures, the NMR spectra were found to broaden significantly and hence various features could not be resolved. These results prove that the nonmagnetic-impurity-induced effects reveal the intrinsic characteristics of

the correlation functions of these systems, both their exponential shape and their extension. Such results were quantitatively explained by Monte Carlo[20–22] and density-matrix renormalization-group simulations.[22–24]

In this paper, we propose to extend such local studies to other impurities, both nonmagnetic and magnetic and to greatly improve the quantitative aspects of these results. We, therefore, present a study of the susceptibility and ^{89}Y NMR spectra on $Y_2BaNi_{1-x}Zn_xO_5$ (YBNO:Zn) and $Y_2BaNi_{1-x}Cu_xO_5$ (YBNO:Cu) ($0 \leq x \leq 0.02$). Dilute concentration of substitutions were preferred in an attempt to observe well-resolved impurity-induced effects on the ^{89}Y NMR spectra far from the impurities and in a temperature regime $T<\Delta$, since the $S=1/2$ excitations interact to a much lesser extent at lower impurity concentrations. We detail the experimental conditions in Sec. II and NMR and bulk susceptibility measurements on YBNO:Zn and YBNO:Cu will be presented in Sec. III. Zn and Cu substitutions are found to induce low-T Curie terms in the bulk susceptibility, while ^{89}Y NMR spectra show a multipeak structure. The multiple peaks are associated to an impurity-induced short-range staggered magnetization which appears very similar for both Zn and Cu. As discussed in Sec. IV, our results on YBNO:Zn prove the universality of the effects of spinless (Mg and Zn) impurities in the $S=1$ chain. These results are quantitatively reproduced by our quantum Monte Carlo (QMC) simulations. Effects of an $S=1/2$ impurity (Cu) are contrasted with those of Zn substitution at various temperatures. Here again, QMC simulations fit the data well and enable us to deduce the magnitude of the exchange coupling between Cu and nn Ni, which is found weak and antiferromagnetic. Finally, the contribution of impurity-induced magnetization to the total susceptibility is extracted from NMR and has been compared to the macroscopic [superconducting quantum interference device (SQUID)] measurements taken on the same set of samples. All results can be well explained in a common VBS-like framework both for Zn and Cu.

II. EXPERIMENTAL DETAILS

Polycrystalline samples of $Y_2BaNi_{1-x}Zn_xO_5$ and $Y_2BaNi_{1-x}Cu_xO_5$ ($0 \leq x \leq 0.02$) were prepared by standard solid-state reaction techniques. Stoichiometric mixtures of predried Y_2O_3, $BaCO_3$, NiO, ZnO, and CuO ($>99.9\%$ pure) were fired in air at 1200 °C. Single-phase samples were obtained after several rounds of grinding, pelletization, and firing. In an attempt to reduce the parasitic Curie term in the susceptibility, as discussed in Sec. III A, we fired the samples in vacuum at 400 °C, in order to reduce the excess oxygen present in the sample. X-ray powder diffraction was carried out using a PHILIPS PW 1729 powder diffractometer, using Si as an internal standard. A Cu target was used in the diffractometer with $\lambda_{av}=1.541\,82$ Å. Lattice parameters were determined from the diffraction pattern using a least-square-fit method. The lattice parameters for the "pure" YBNO sample were found to be 3.763(1) Å, 5.762(1) Å, and 11.334(3) Å along a, b, and c axes, respectively, which are in agreement with the earlier results.[8] The lattice parameters remain almost unchanged after Zn and Cu substitution.

The nearly identical effective ionic radii[25] of Ni^{2+}, Zn^{2+}, and Cu^{2+} together with the dilute level of doping may be the cause of the unchanged lattice parameters.

Magnetization M measurements were performed as a function of temperature T (1.8 K$\leq T \leq$ 300 K) and an applied field H (0$\leq H \leq$ 50 kG) using a SQUID magnetometer.

NMR measurements were performed by standard pulsed NMR techniques in an applied field $H_0 = 70$ kG at different temperatures (50 K$\leq T \leq$ 325 K). The typical width of the applied $\pi/2$ pulse was $t_W = 6$ μs. The line shape was obtained by Fourier transform of the NMR echo signals. The ^{89}Y NMR shift $K(T) = [\nu(T) - \nu_{ref}]/\nu_{ref}$ was measured with respect to a standard YCl$_3$ solution [$\nu(T)$ is the resonance frequency of Y$_2$BaNiO$_5$ at different temperatures and $\nu_{ref} = 14\,594.15$ kHz is the resonance frequency of YCl$_3$ in our experiment]. At higher temperatures (120 K$\leq T \leq$ 300 K), the spectral width of the $\pi/2$ pulse was sufficient to reliably obtain the full spectrum. However, at lower temperatures ($T < 120$ K), where the multiple resonance lines are spaced far apart in frequency, we varied the irradiation frequency to obtain the full spectrum as the spectral width of the single $\pi/2$ pulse was insufficient.

The quantum Monte Carlo simulations were performed using the stochastic series expansion method,[26,27] with generalized directed loop techniques.[28–30] Calculations of magnetization profiles were done for long runs of about 2×10^8 Monte Carlo steps for an isotropic $S=1$ Heisenberg model, with an imposed magnetic field of about 70 kG, corresponding to the field used in the NMR experiments.

III. RESULTS

A. Bulk susceptibility

Susceptibility $\chi(T)$ of Y$_2$BaNi$_{1-x}$Zn$_x$O$_5$ and Y$_2$BaNi$_{1-x}$Cu$_x$O$_5$ ($0 \leq x \leq 0.02$) was measured as a function of T in an applied field of $H = 5$ kG (Fig. 2). We checked for the possible presence of spurious ferromagnetic impurities by measuring M versus H isotherms at different temperatures in order to separate the linear (paramagnetic) and nonlinear (ferromagnetic) contributions. The ferromagnetic contribution corresponds to about 2 ppm of ferromagnetic Fe impurity which amounts to at most 0.2% of the susceptibility. It is, hence, neglected in our analysis. The paramagnetic susceptibility for the pure sample is in rough agreement with the results published earlier.[14,31] The susceptibility decreases as $e^{-\Delta/T}/\sqrt{T}$ with decreasing temperature, as a consequence of the Haldane gap.[32] At lower temperatures ($T < 50$ K), there is a Curie-Weiss-like $C/(T + \theta)$ upturn in the susceptibility. This parasitic Curie term in the pure sample might presumably result from various sources such as natural chain breaks, presence of Ni^{3+} (as a result of small oxygen nonstoichiometry), and extrinsic paramagnetic phases present in the sample. A substantial reduction in this low-T contribution to the susceptibility (i.e., reduction in the Curie term C) was achieved by vacuum annealing the powders at 400 °C, as evident from the inset of Fig. 2(a). A similar reduction in the parasitic Curie term in a $S = 1/2$ chain compound, Sr$_2$CuO$_3$, was observed earlier by Ami *et al.*[33] after annealing in inert

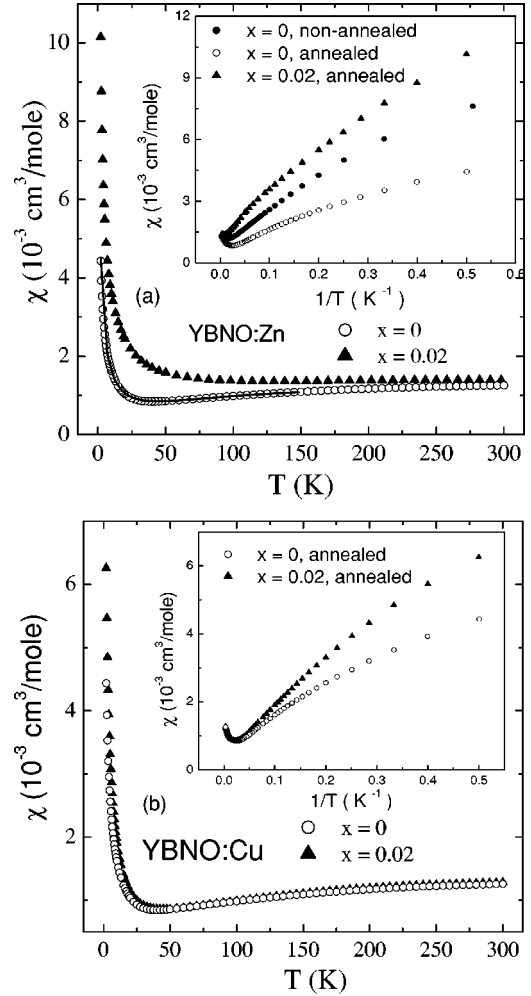FIG. 2. Magnetic susceptibility vs temperature T for (a) Y$_2$BaNi$_{1-x}$Zn$_x$O$_5$ and (b) Y$_2$BaNi$_{1-x}$Cu$_x$O$_5$ ($0 \leq x \leq 0.02$). The solid line follows Eq. (5) and the fitting was done using the procedure discussed in Sec. IV C, for the "pure" YBNO sample for $T < 150$ K. In the insets, the representation vs $1/T$ evidences the Curie law behavior at low temperatures. Comparison between nonannealed and annealed samples in the inset of (a) shows that annealing leads to a reduction of the Curie term. In contrast, Zn or Cu substitution leads to an increase of the Curie term.

atmosphere. Reduction in the Curie term in our samples might be due to removal of excess oxygen leading to a reduction in the amount of Ni^{3+} due to the above process. A discussion about intrinsic defects, effect of vacuum annealing, and the implications on SQUID and NMR measurements is carried out in Sec. IV D. All measurements with the substituted samples reported hereafter are on the vacuum annealed samples. In case of the substituted samples, the susceptibility at lower temperatures increases with increasing dopant content [shown in Figs. 2 (a,b), inset], which indicates an increase in the Curie term for the substituted samples.

B. ^{89}Y NMR

In YBNO, each ^{89}Y has two nn Ni^{2+} from one chain and two next-nearest-neighbor (nnn) Ni^{2+} from two different
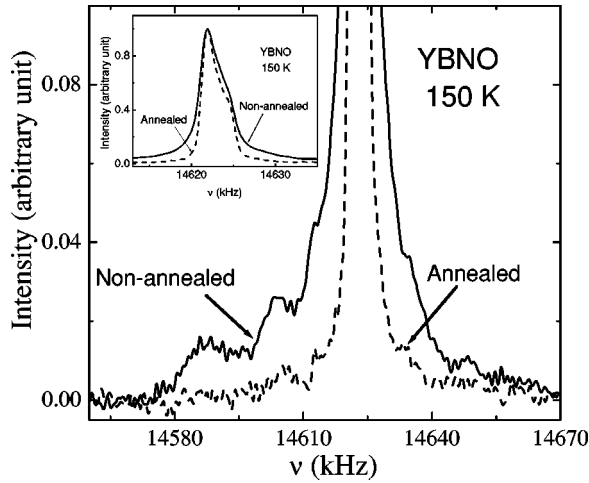
FIG. 3. Comparison of the [89]Y NMR spectra of the nonannealed and annealed YBNO at 150 K (in the inset, the full line and in the main frame, a vertical zoom). The intensity of the satellite peaks reduce after vacuum annealing showing that the corresponding defects are eliminated by annealing.

FIG. 4. [89]Y NMR shift of the mainline [89]K as a function of temperature T, for pure (present results and from Shimizu *et al.* (Ref. 14)) and substituted samples. [89]$K(T)$, which measure the uniform susceptibility, remains unaffected by substitutions. The solid line represents a fit to Eq. (1) for the Cu doped sample and is discussed in detail in Sec. IV A.

chains [Figs. 1 (a,b)]. However, [89]Y is actually coupled to the Ni^{2+} spins belonging to nnn chains, not to the nn one. Indeed, there is no appreciable exchange between Y and Ni $3d$ or oxygen p orbitals belonging to nn chain. In contrast, there is an appreciable overlap between the nnn-oxygen p_π orbital with the $5s$ orbital of Y^{3+} and hence with the nnn Ni-O-Ni chains.

We performed [89]Y NMR on the pure and substituted samples at different temperatures. In case of the annealed and nonannealed pure samples, we observed one asymmetric central peak (inset Fig. 3) shifted from ν_{ref} in the Fourier-transformed spectrum, together with less intense peaks (satellites) on both sides of the central peak (see Fig. 3). The shift in the [89]Y NMR peak of the pure YBNO arises from the coupling of Y nuclei to Ni^{2+} spins of two different nnn chains. Since our measurements are on randomly aligned polycrystalline samples, asymmetric line shape of the central peak (mainline) in the annealed sample corresponds to a powder pattern due to an asymmetric hyperfine coupling tensor A_{hf}[14] and anisotropic susceptibility.[11] The vacuum annealing procedure leads to a large narrowing of the mainline and a decrease of the satellites intensities. The amount of defects corresponding to these satellites can be determined by measuring their area. Using an asymmetric Lorenzian fit, the fractional area of one of these satellites decreases from 3.2% to 0.8% after annealing. These satellites in pure YBNO presumably originate from the in-chain defects, which will be discussed in details in Sec. IV D.

In substituted compounds, the shift of the mainline $K(T)$ remains unchanged from the pure sample at different temperatures (Fig. 4) and compares well with the results published earlier.[14] This implies that the Haldane gap remains the same after impurity substitution. In contrast, the introduction of impurities (Zn/Cu) at the Ni site of the chain results in a change in the local environment of the impurity. This change is evident by the appearance of satellites on both sides of the mainline. For example, in Fig. 5, we compare the
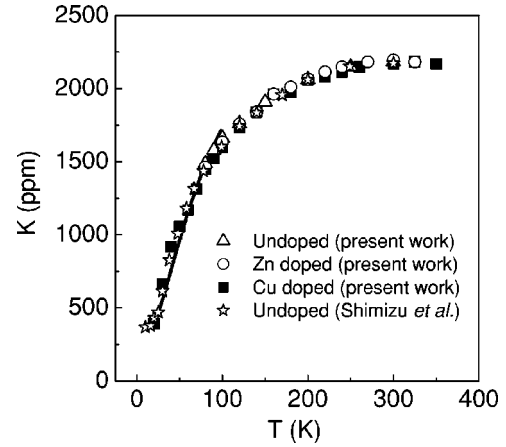
NMR spectra of pure, 0.5% Zn and 2% Zn substituted samples at 120 K [Fig. 5 (a)] and 0.5% Cu and 1% Cu substituted samples at 300 K [Fig. 5 (b)]. The intensity of the impurity-induced satellites increases with increasing impurity concentration keeping their shift from the mainline constant. This establishes that the satellite peaks are a direct consequence of substitutions and their positions are independent of their concentration, i.e., of the length of the chains. Furthermore, fractional intensities of these Cu- and Zn-induced satellites are significantly larger than the weak satellites observed in the annealed pure sample. Hence, they can safely be attributed to Zn or Cu neighbors. Each of these satellites represents [89]Y nuclei at a given distance from the impurity. Since one Y nucleus is coupled to two different nnn chains [see Fig. 1(b)], for a concentration x of the impurity, there should be $4x$ Y nuclei contributing to each satellite. Using an asymmetric Lorenzian fit (Fig. 6), we extracted the fractional area of one satellite peak with respect to the whole spectrum (outermost satellite on the right side of the mainline, marked by 1 in Fig. 6). For a nominal concentration $x = 2\%$ of Zn or Cu, our fit leads to an effective concentration of $(1.9 \pm 0.1)\%$ for Zn and $(1.8 \pm 0.2)\%$ for Cu. This good agreement between the nominal stoichiometry and the actual in-chain number of defects shows that the substitution amount is well controlled here.

Comparison of Cu and Zn [89]Y NMR spectra done in Fig. 7 shows that Cu induces a staggered magnetization like Zn. But the difference in the shifts of the NMR satellites shows that the amplitude of the induced magnetization near Cu is smaller than that for Zn. Representative [89]Y spectra are shown at different temperatures in Figs. 8(a) and 8(b) for 2% Zn and 0.5% Cu substituted samples, respectively. The Ni^{2+} ions closest to the impurity are the most affected by the substituent and give rise to the most shifted satellite indexed as the first neighbor [1 in Figs. 8(a) and 8(b)]. Further satellites are numbered in accordance with their decreasing shifts with respect to the mainline. Satellites with decreas-
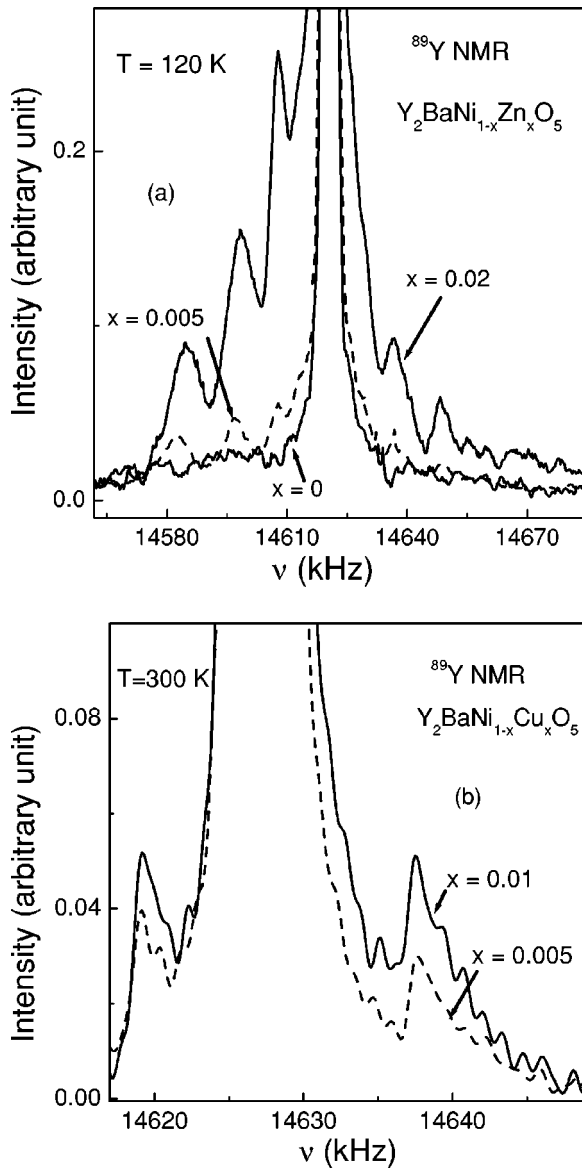
FIG. 6. First- and third-neighbor satellite peaks (labeled 1 and 3) for $Y_2BaNi_{0.98}Zn_{0.02}O_5$ and $Y_2BaNi_{0.98}Cu_{0.02}O_5$ at 200 K (solid lines) and fit of satellite 1 using an asymmetric Lorenzian line shape (dotted lines).

satellite has been observed clearly in Fig. 8(a) where it is labeled as 0: it is half as shifted as the mainline and half as intense as the other satellites. In the case of YBNO:Cu, such a peak is not observed as seen in Fig. 8(b). This is not surprising as the $S=1/2$ Cu spin will now contribute to its shift, which should now become large, and would be severely affected by a large spin-lattice relaxation rate. Therefore, the absence of such a peak is a clear local evidence that Cu has indeed successfully substituted at a Ni site.

The shifts of the observed satellites were measured for different temperatures and concentrations. Since for $T < 100$ K, the outer satellites lie outside the spectral width of the rf pulse, data were taken at various irradiation frequen-

FIG. 5. (a) Expanded view of the satellites of the ^{89}Y spectra of $Y_2BaNi_{1-x}Zn_xO_5$ $(0 \leq x \leq 0.02)$ at 120 K. Intensity of these satellites increases with increasing Zn content. The positions of the satellite peaks are independent of the Zn concentration. (b) Comparison of the satellites for 0.5% and 1% Cu substitution at the Ni site at 300 K. The satellite intensity increases linearly with Cu content.

ing shifts alternate on each side of the mainline. This shows that the corresponding Ni sites have a magnetization, which alternates in sign in addition to the nonperturbed magnetization represented here by the mainline shift. The appearance of such induced staggered magnetization near the defects is indeed expected by theoretical computations,[21,22] as will be quantitatively detailed hereafter.

In the case of Zn, the nearest Y nuclei to the impurity [marked by 0 in Fig. 1(b)] couple to both Zn itself and one undisturbed chain. Therefore, its corresponding NMR line should be shifted by half of that of the mainline with respect to ν_{ref}, as Zn is nonmagnetic and hence does not contribute to K. Furthermore, this satellite should be half the intensity of the other satellites, from its specific position. In fact, this
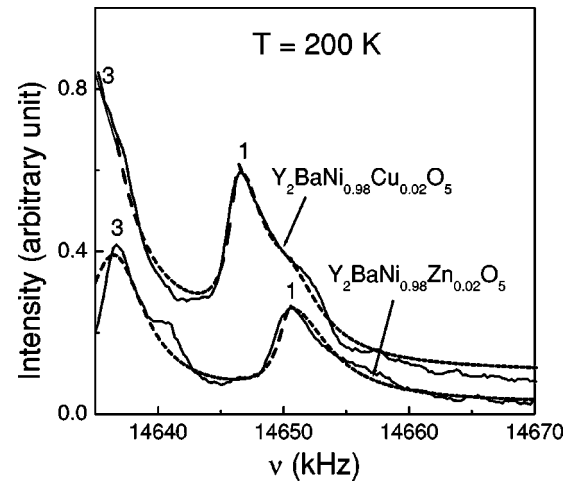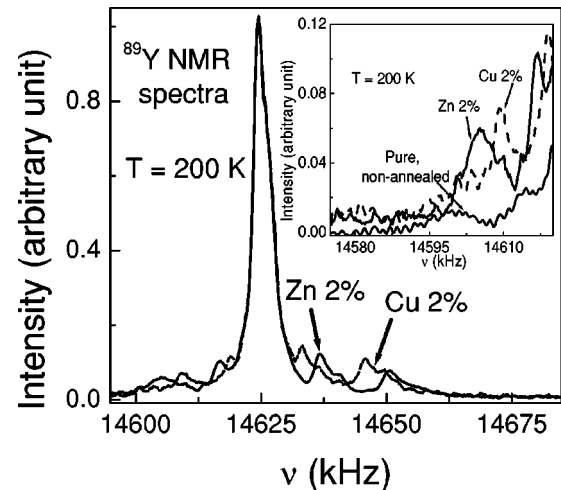

FIG. 7. Comparison of ^{89}Y NMR spectra of $Y_2BaNi_{0.98}Zn_{0.02}O_5$ and $Y_2BaNi_{0.98}Cu_{0.02}O_5$ measured at $T = 200$ K. The mainline position is the same for both substitutions. The satellites for the Cu substitution are less shifted than those for Zn. Inset: Position of the satellite peaks on the lower-frequency side of the mainline for nonannealed pure YBNO, $Y_2BaNi_{0.98}Zn_{0.02}O_5$ and $Y_2BaNi_{0.98}Cu_{0.02}O_5$ at 200 K.
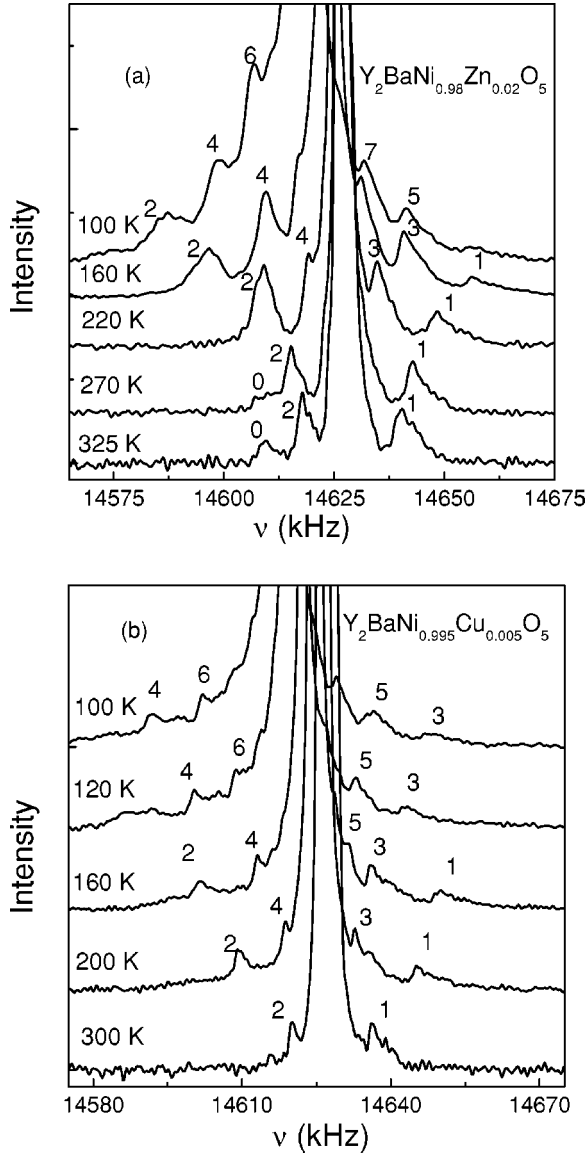
FIG. 8. ^{89}Y NMR spectra of (a) $Y_2BaNi_{0.98}Zn_{0.02}O_5$ and (b) $Y_2BaNi_{0.995}Cu_{0.005}O_5$ at different temperatures. Satellite peaks are indexed in accordance with their decreasing shift from the mainline and with the position of the ^{89}Y labeled in Fig. 1(b). The peak originating from the Y neighbor to the Zn impurity (as discussed in Sec. III B) is marked by 0 in (a).

cies to reliably determine their peak positions from the Fourier transforms. These data are not shown in Fig. 8. We note the shifts of the ith satellite as $\delta\nu_i = \nu_i - \nu_{main}$, where ν_i and ν_{main} are frequencies corresponding to its center of gravity and that of the mainline, respectively. Due to the asymmetric powder pattern shapes, consideration of the center of gravity for each peak yields a better description of the impurity-induced effects in the chain. In Fig. 9(a), we present these shifts of the satellites ($\delta\nu_i$) at various temperatures for the spinless Zn impurity. On the same figure, we plot as well the data published earlier for the Mg impurity, which is found identical to that of Zn.[17] Therefore, the induced magnetization by both Zn and Mg is quantitatively the same. In the present study, the use of samples with smaller impurity con-
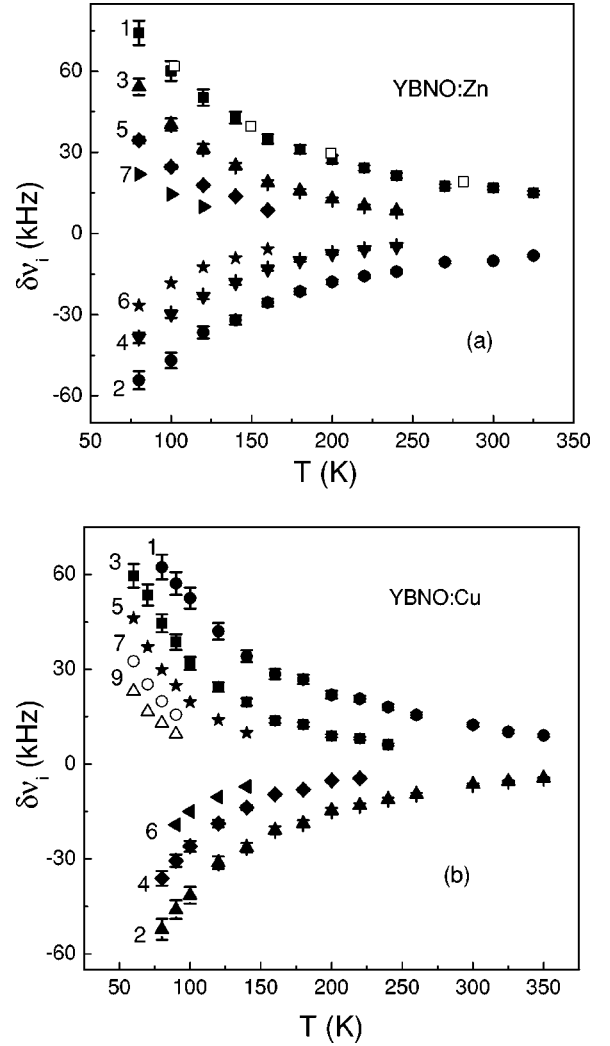

FIG. 9. Temperature dependence of $\delta\nu_i$, the frequency shift of the different satellites with respect to the central line for (a) YBNO:Zn and (b) YBNO:Cu. The open squares in (a) represent the shifts obtained in Ref. 17 for YBNO:Mg. At lower temperatures, the broadening of the NMR spectra restricted us from obtaining satellite shifts with high resolution. Indices represent the ith neighbor to the impurity in accordance with Fig. 1(b).

tent and less natural defects allowed us to largely improve the resolution and to detect more satellites in a wider temperature range. A similar plot is shown in Fig. 9(b) for YBNO:Cu. These measurements allow us to get a direct measure of the amplitude and spatial shape of the magnetization induced by both nonmagnetic and magnetic impurities, as will be discussed later.

IV. DISCUSSION

A. Determination of the parameters of the Haldane Hamiltonian of the pure system

The bulk susceptibility $\chi(T)$ in the pure YBNO contains the contribution from some unknown defects and extrinsic paramagnetic phases in addition to the intrinsic gap contribution. On the other hand, in ^{89}Y NMR spectra, defects and

intrinsic behavior can be easily distinguished since defects broaden the mainline or induce satellites, whereas the intrinsic behavior is measured by the mainline shift. Hence, the T dependence of the "gap term" is best reflected by the temperature dependence of the NMR shift $K(T)$.

Indeed, the NMR shift $^{89}K(T)$ of the central line is expected to vary linearly with the uniform susceptibility $\chi_u(T)$ through

$$K(T) = \frac{2A_{hf}}{\mu_B N_A} \chi_u(T) + K(0). \tag{1}$$

Here, A_{hf} is the ^{89}Y - Ni hyperfine coupling constant and is independent of temperature, N_A is the Avogadro number, and $K(0)$ is the chemical shift independent of temperature. The NMR shift $K(T)$ results from two nnn chains, while $\chi_u(T)$ represents the intrinsic susceptibility of one $S=1$ chain, which explains the factor 2. As reported in Fig. 4, the shift $K(T)$ of the central peak decreases with decreasing T and remains unchanged for all the samples at the corresponding T. The observed exponential decrease in $K(T)$ at low T is direct evidence of the presence of the Haldane gap. Our measurements on different samples at different temperatures match well with earlier results of Shimizu *et al.* for pure YBNO (Ref. 14) (as shown in Fig. 4). This indicates that the gap remains unchanged for impurity substituted samples. Affleck showed that the low-temperature part of the susceptibility should follow $\sqrt{(\Delta/T)}e^{-\Delta/T}$.[32] Previous studies used this model to fit the low-T part of both NMR and macroscopic susceptibility measurements in order to extract the Haldane gap and the superexchange coupling J. This model also fits our data, as shown by a solid line in Fig. 4 for the Cu 0.5% compound, leading to $K(0)=340$ ppm and $\Delta=(88 \pm 7)$ K, which is in good agreement with the results published earlier.[13,14]

However, we propose here a more rigorous way to determine J. We used QMC simulations to directly fit our data in the full temperature range. We have calculated theoretically, by QMC simulations, the uniform susceptibility χ_u versus T/J, i.e., the susceptibility of the infinite $S=1$ chain theoretically, by QMC simulations. The shift K obtained from our NMR experiments has then been plotted versus this χ_u for different J values in Fig. 10 with T as an implicit parameter. The $T\rightarrow 0$ value of K is constrained by Shimizu's NMR measurements,[14] which allowed to accurately determine $^{89}K(T\rightarrow 0)=370 \pm 10$ ppm, a value compatible with our measurements. Using this constraint, a good linear fit is obtained for $J=250 \pm 10$ K (shown by the solid line). This proves that the uniform susceptibility measured by NMR is well accounted by QMC simulations up to $T=350$ K. This procedure of determining J allows for a much sharper constraint on the determination of J than the previous determinations. We believe that this procedure enables the determination of J to be more reliable than before. The corresponding theoretical Haldane gap[34] would be $\Delta=0.41J=102 \pm 4$ K, a value compatible with our first rough estimate and with the previous experiments.[11] This fitting method also allows a determination of the hyperfine coupling A_{hf} independent of any macroscopic susceptibility measure-
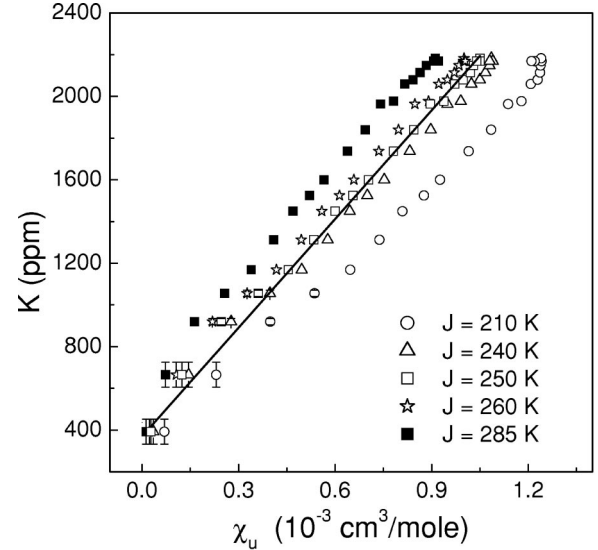

FIG. 10. ^{89}Y NMR shift of the central line K as a function of χ_u computed by QMC using different J values (with T as an implicit parameter). The solid line represents the best linear fit and allows to determine both J and the hyperfine coupling constant A_{hf} [using the constraint $K(0)=370 \pm 10$ ppm as detailed in the text].

ment. We performed similar fitting for all substituted and pure YBNO shifts plotted in Fig. 10. This leads to $A_{hf}=(4.7 \pm 0.2)$ kG/μ_B. This value should be more reliable than earlier determinations done by Shimizu *et al.*[14] ($A_{hf}=4.9$ kG/μ_B) and by Tedoldi *et al.*[17] ($A_{hf}=6.5$ kG/μ_B), which relied too much on the actual measurements of the susceptibility of the pure compound, as this measurement is always hampered by the large low-temperature Curie contributions.[35]

B. Impurity-induced staggered magnetization

1. Spatial dependence of the induced staggered magnetization

In Figs. 11(a) and 11(b), we depict the site dependence of $|\delta\nu_i(T)|$ at different temperatures for YBNO:Zn and YBNO:Cu, respectively, on a logarithmic scale. At a given T, the observed linear behavior shows that $|\delta\nu_i(T)|$ varies exponentially as a function of distance from the impurity. In fact, the shifts can be fitted at all temperatures for both Cu and Zn by

$$|\delta\nu_i(T)| = |\delta\nu_1(T)| e^{-(i-1)/\xi_{imp}(T)}. \tag{2}$$

Here $\xi_{imp}(T)$ is the extension of the impurity-induced staggered magnetization. The values of $\xi_{imp}(T)$ extracted from our measurements are represented in Fig. 12 and compared with those obtained by Tedoldi *et al.* in the case of Mg substitution.[17] It clearly appears that Cu, Zn, and Mg induce a staggered magnetization with the same spatial extent. Furthermore, this spatial extent $\xi_{imp}(T)$ is found almost identical to the correlation length computed for an infinite $S=1$ chain with no defects.[34] The experimental values of $\xi_{imp}(T)$ are systematically found about 5% higher than the values of $\xi(T)$ (Ref. 34), but this discrepancy is still within experimental accuracy (e.g., at 200 K, $\xi_{imp}=2.5 \pm 0.2$, while ξ
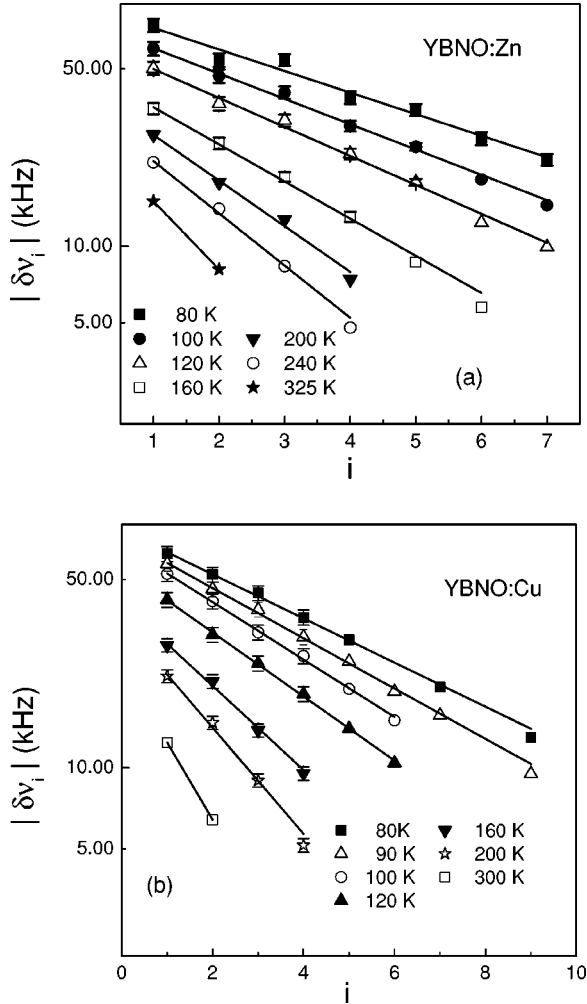
FIG. 11. Site dependence of the impurity-induced magnetic shift $|\delta\nu_i|$ at different temperatures for (a) YBNO:Zn and (b) YBNO:Cu. The log-scale representation evidences that $|\delta\nu_i|$ is exponentially decaying. The solid lines are fits to the exponential relation represented by Eq. (2).
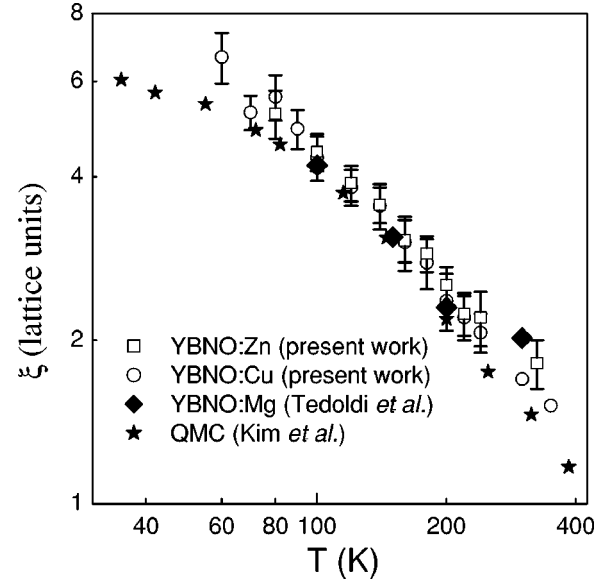

FIG. 12. Comparison of $\xi_{imp}(T)$ obtained from our experiments from Eq. (2) and Fig. 11 for YBNO:Zn, YBNO:Cu , for YBNO:Mg by Tedoldi *et al.* (Ref. 17), and for the infinite chain correlation length $\xi(T)$ calculated by QMC by Kim *et al.* (Ref. 33).

$=2.3$). The lowest-temperature data, which were only taken in the case of Cu impurities, depart a little bit more from the value of $\xi(T)$. The good agreement found shows that for both $S=0$ and $S=1/2$ impurities, the characteristic length of the staggered magnetization near defects reveals indeed the intrinsic $\xi(T)$ of the infinite $S=1$ chain, in the explored temperature range.

2. Comparison with QMC for Zn and Cu

For both $S=0$ (Zn) and $S=1/2$ (Cu) impurity, we compared our experimental results to those predicted by QMC calculations for the local susceptibility around impurities. As discussed earlier, the total magnetization M_i at the ith site in the chain is the sum of the uniform magnetization and the impurity-induced magnetization, i.e., $M_i = g\mu_B\langle S_z^i\rangle$ $= g\mu_B(\langle S_z\rangle_u + \delta\langle S_z^i\rangle)$. We can determine directly, from the NMR data for $\delta\nu_i$ and the mainline shift, the ratio of the impurity-induced staggered magnetization and uniform magnetization $\delta\langle S_z^i\rangle/\langle S_z\rangle_u$, using the value of $K(0)=340$ ppm

deduced from Figs. 4 and 10. This experimental quantity could be directly compared with that computed by QMC simulation for the spatial dependence of the spin polarization at chain ends.

In case of the $S=0$ impurity, we performed such QMC calculations considering $J=230$ K, 250 K, and 270 K at $T=100$ K. The computed impurity-induced staggered magnetization decays exponentially away from the impurity as in the experimental results, following Eq. 2 [Fig. 13(a)]. The computed extension ξ_{imp} matches well with the previous results[34] considering $J=270$ K. Further, we found that the experimental ratio of the impurity-induced staggered magnetization and uniform magnetization match well with QMC for $J=270\pm10$ K as shown in Fig. 13(a). This value of J is consistent with the one independently determined from the uniform susceptibility far from the defect $J=250\pm10$ K. This proves the coherence of our analysis, as the same coupling J can account both for the susceptibility of the pure compound, and for the shape, amplitude, and extension of the induced magnetization near spinless defects. The determination of A_{hf} enables us to convert the NMR shifts into absolute magnetization values. Here, we have calculated $\langle S_z^i\rangle_{Zn}$, from our experimental data using the relation $\langle S_z^i\rangle = 2\pi[2\nu_i - (\nu_{ref} + \nu_{main})]/2\gamma g A_{hf}$. Here, $\gamma/2\pi = 2.0859$ MHz/T is the [89]Y gyromagnetic ratio and g is the Landé g factor. The temperature dependence of $\langle S_z^i\rangle$ is also well fitted by the QMC simulations as exemplified in Fig. 13(b).

In case of the $S=1/2$ substitution, theoretical calculations were done earlier to predict the behavior of $S=1/2$ impurity in $S=1$ chain.[23,36,37] The $S=1/2$ impurity is modeled by considering that its coupling J' to its near-neighbor Ni can be different from J. We have performed QMC calculations for various J' ranging from $-J$ to $+J$. The magnetic impu-
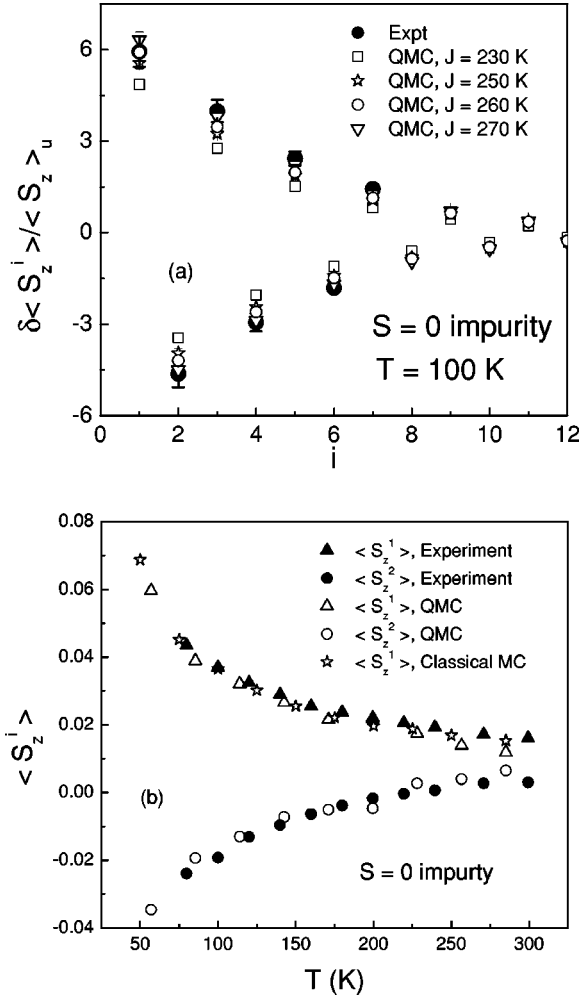
FIG. 13. (a) Comparison at $T=100$ K of the spatial dependence of the staggered magnetization $\delta\langle S_z^i\rangle/\langle S_z\rangle_u$ for YBNO:Zn with the corresponding QMC simulations for various J values, which shows a good agreement for $J=270\pm10$ K. (b) Comparison of the T variation of the magnetization $\langle S_z^i\rangle$ of the first and second neighbor ($i=1$ and 2, respectively) with the QMC calculations. Filled symbols represent our experimental data while open triangles and circles represent our QMC results for $J=260$ K. The open stars are the results of classical Monte Carlo calculations (Ref. 19).

rity is found to induce a staggered magnetization as in the spinless case. Furthermore, its extension is found identical for temperatures higher than J'. These results are then in perfect agreement with our data. For $T>J'$, the only change, which begins to appear when comparing the $S=1/2$ and $S=0$ induced effects in QMC results, is the amplitude of the staggered magnetization. We found that for a ferromagnetic coupling of the impurity to the nn Ni ($J'<0$), the staggered magnetization on the first, second, and further neighbors is larger than that for a nonmagnetic impurity. In contrast, an antiferromagnetic coupling ($J'>0$) leads to a smaller magnetization. The experimentally observed $\delta\nu_i$ for YBNO:Cu is less than that for YBNO:Zn ($J'=0$) at the corresponding temperature, as exemplified in Fig. 7. This strongly suggests that the Cu-Ni coupling is then antiferromagnetic. A quantitative comparison between QMC results and experiments en-
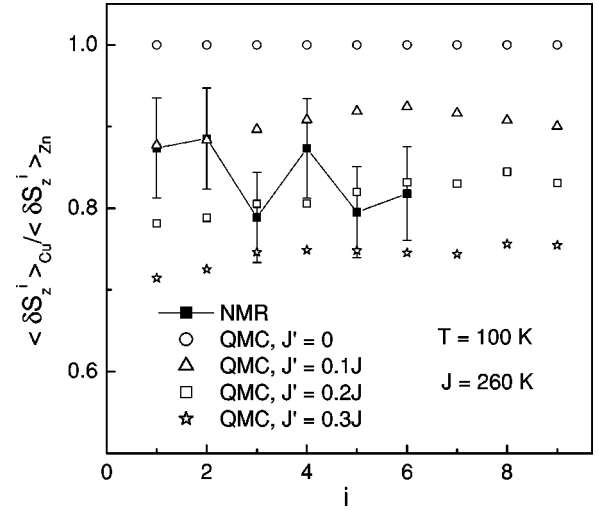

FIG. 14. Spatial dependence of the experimental ratio $\langle\delta S_z^i\rangle_{\mathrm{Cu}}/\langle\delta S_z^i\rangle_{\mathrm{Zn}}$ of the staggered magnetization near Cu to that near Zn. The data are compared to QMC simulations for various values of the Heisenberg coupling J' between Cu and its nn neighbors Ni at $T=100$ K.

ables us to deduce J'. In Fig. 14, we compared the experimental ratio $(\delta\nu_i)_{\mathrm{Cu}}/(\delta\nu_i)_{\mathrm{Zn}}$ to that theoretically obtained for $\langle\delta S_z^i\rangle_{\mathrm{Cu}}/\langle\delta S_z^i\rangle_{\mathrm{Zn}}$ for different values J'/J. The experimental and theoretical results match well for $0.1J\leq J'$ $\leq0.2J$, which allows us to deduce an estimate $J'=(0.15 \pm0.05)J$.

3. Determination of the total induced susceptibility

The magnetization induced by impurities can be written as $\delta M_i=g\mu_B\delta\langle S_z^i\rangle$, where $\delta\langle S_z^i\rangle=2\pi\delta\nu_i/\gamma g A_{hf}$. This conversion enables us to deduce from NMR the contribution of substituted impurities χ_{imp}^{NMR} to the macroscopic susceptibility. As the impurity-induced magnetization decays exponentially as a function of site on either side of the impurity in the 1D chain, χ_{imp}^{NMR} can be expressed as

$$\chi_1(T)=\frac{\delta M_1(T)}{H_0}, \qquad (3)$$

$$\chi_{imp}^{NMR}(T)=\frac{2xN_A\chi_1(T)}{100}\sum_i(-1)^{i-1}e^{-(i-1)/\xi_{imp}(T)}. \qquad (4)$$

Here, $\chi_1(T)$ is the impurity-induced susceptibility on the first neighbor to the impurity and N_A is the Avogadro number, x is the amount of impurities per Ni in percent. The variation of $\chi_{imp}^{NMR}(T)$, shown in Fig. 15, can be fitted to $\chi_{imp}^{NMR}(T)=C^{NMR}/T$. From the fit, we get $C_{\mathrm{Zn}}^{NMR}=(5.6\pm0.6)\times10^{-3}$ cm^3 K/mole/% Zn and $C_{\mathrm{Cu}}^{NMR}=(4.7\pm0.5)\times10^{-3}$ cm^3 K/mole/% Cu. These Curie terms lead to the corresponding spin value S on each side of the impurity through $C=2N_A g^2 S(S+1)\mu_B^2/3k_B$. For Zn, one finds an impurity-induced "effective spin" $S=0.4\pm0.06$ on either side of the impurity in the chain, which is close to the VBS
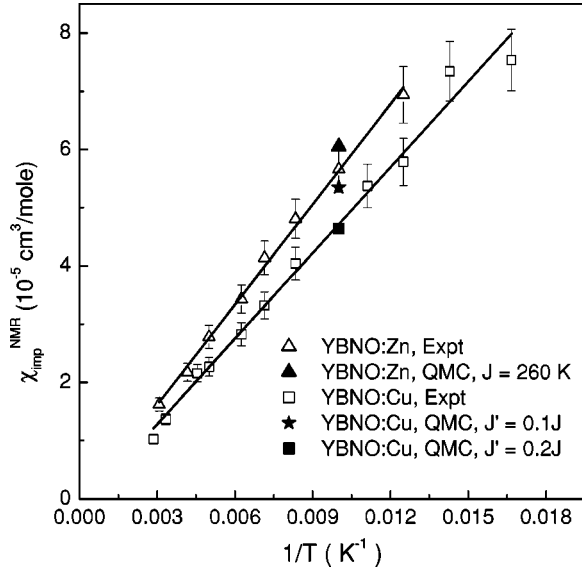
FIG. 15. The impurity-induced total susceptibility $\chi_{imp}^{NMR}(T)$ estimated from NMR data is plotted vs $1/T$ for YBNO:Zn$_{1\%}$ (open triangles) and YBNO:Cu$_{1\%}$ (open squares). The solid lines represent the Curie-like fits to $\chi_{imp}^{NMR}(T)$. The solid symbols represent the values obtained at 100 K from the corresponding QMC simulations.

predicted $S=0.5$. In case of YBNO:Cu, as χ_{Cu}^{NMR} is also found to follow a Curie behavior, the impurity-induced susceptibility on either side of the impurity behaves almost as a free spin in the explored T range. The lower value of C_{Cu}^{NMR} than C_{Zn}^{NMR} is well accounted for, here again, by QMC simulations, if the Cu spin couples weakly and antiferromagnetically to the nearest-neighbor Ni spin.

C. Temperature dependence of the macroscopic susceptibility

As already stressed, the macroscopic susceptibility presented in Fig. 2 results from distinct contributions: the uniform contribution $\chi_u(T)$ which exhibits the Haldane gap which decreases exponentially with decreasing temperature; the intrinsic defects such as Zn or Cu, and the other unknown defects and paramagnetic species, which are already present in the pure compound. The latter two contributions mainly give rise to a Curie-like magnetization in the low-temperature region. We plotted these different contributions in the case of pure YBNO in Fig. 16. Note that the total susceptibility not only consists of the Haldane term and a Curie term, but also includes a residual non-Curie term, which could be due to some defects that are not purely paramagnetic. This small residual non-Curie term exists in all our samples, as evidenced in Fig. 17 and does not show any obvious connection with the substitution. It, therefore, limits any quantitative analysis of the substitution effect on macroscopic susceptibility. Furthermore, the large contribution of the Curie term present at low T even in the pure compound also severely limits any analysis, contrary to NMR experiments for which the Zn and Cu effects could be isolated. However, at low temperatures, the total susceptibility can be tentatively modeled by
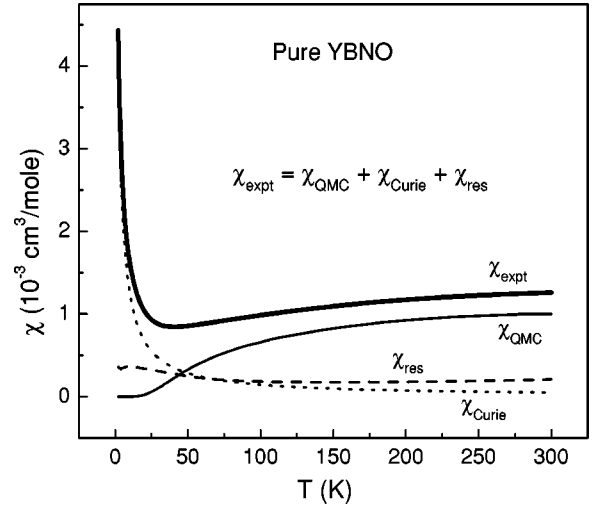

FIG. 16. Macroscopic susceptibility of pure YBNO and its decomposition into a sum of three terms: the QMC computed (Haldane gap related) decrease of the uniform susceptibility for $J = 260$ K, a Curie term extracted from a fit to the data for $T < 30$ K, and the residual part which cannot be accounted for by the two preceding forms.

$$\chi_{SQUID}(T) = \chi_0 + \frac{C^{SQUID}}{T+\theta} + \chi_u(T). \qquad (5)$$

Here, χ_0 is the constant term, which originates from Van Vleck paramagnetism and core diamagnetism, C^{SQUID} is the Curie constant. As discussed in the previous sections, the determination of the superexchange coupling $J = 260 \pm 10$ K allows us to determine independently $\chi_u(T)$ by using the QMC simulation results, which fit perfectly the mainline NMR data. In order to estimate the Curie constant C and θ reliably, we therefore fitted $\chi_{SQUID}(T)$ for the substituted as well as the pure samples to Eq. (5) in the temperature range
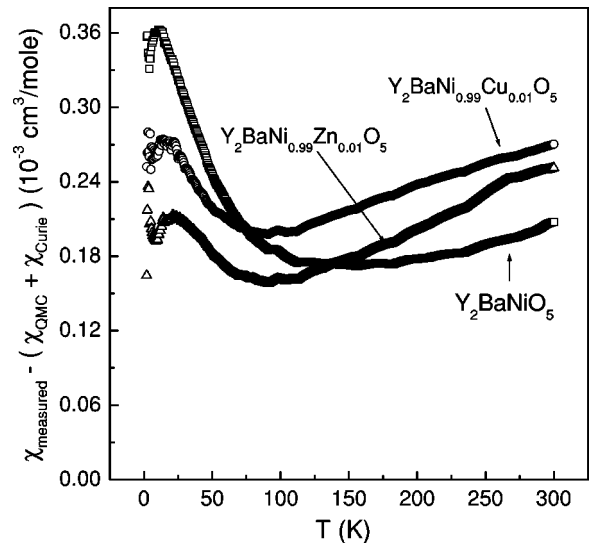

FIG. 17. The residual terms deduced from the macroscopic susceptibility analysis detailed in the text and in Fig. 16 are compared here for various samples.

2 K$\leqslant T\leqslant$25 K. We then fit our susceptibility data (T $<$150 K) for all the samples to extract the values of χ_0 keeping the value of C and θ obtained from the low-temperature fit. From the fit [shown by solid line in Fig. 2(a)], we found that χ_0 remains almost unchanged for all the samples (χ_0 $\approx 0.3\times10^{-3}$ cm^3 K/mole). A small $\theta\approx1$ K fits the data reliably for all the samples.

D. Comparison of NMR and macroscopic susceptibility in pure YBNO: Nature of intrinsic defects

Comparison of NMR and SQUID measurements in pure nonannealed and annealed samples allows us to get a better understanding of the various types of defects present in the pure YBNO. The annealing procedure leads to a reduction of the Curie term C^{SQUID} from 25.4×10^{-3} cm^3 K/mole to 13.7×10^{-3} cm^3 K/mole. Such reduction shows that annealing cures part of the defects in the compound. The corresponding ^{89}Y NMR spectra of the nonannealed and annealed compounds are presented in Fig. 3. In the nonannealed sample, satellite peaks observed at frequencies smaller than the central peak are of higher intensity than those noticed on the higher-frequency side. After annealing, the intensity of the satellites reduced on both sides of the central peak and the intensity of the left side satellites almost equals to those in the right side of the mainline. Hence, there are probably various kinds of defects: in-chain defects which give rise to satellites exactly like Zn would do, and other defects which lead to the broad low-frequency feature. There must be also magnetic entities at other nonchain sites, which do not affect the ^{89}Y NMR signal, since SQUID data show a large residual Curie term in the annealed compound. The in-chain defects could be chain breaks, due to the polycrystalline nature of the sample, vacancies at Ni site and presence of Ni^{3+} in the chain. The other defects could be Ni^{3+} in the interstitial places. Presumably, annealing in vacuum reduces the quantity of chain breaks (some Ni ion might migrate to the vacant sites on annealing at 400 °C) and Ni^{3+} in the sample, which is responsible for the reduction of satellite intensity. Annealing results in a reduction from 0.8%/Ni to 0.2%/Ni of in-chain defects. If one assumes that each of these in-chain defects is giving rise, as in the Zn case, to two S $=1/2$ spins at low T, the reduction of 0.6% of defects in the chain by annealing should lead to a decrease in the Curie constant of 4.5×10^{-3} cm^3 K/mole ($0.6\times2\times3.75$ $\times10^{-3}$ cm^3 K/mole). Our observed reduction in Curie constant was higher than this by 7.2×10^{-3} cm^3 K/mole. So the annealing not only reduces the chain defects but might also reduce the number of Ni^{3+} (present in YBNO) or remove some of the excess oxygen present in the other extrinsic paramagnetic phases (say, BaNiO$_{2+x}$). Some of these defects are, however, still present in smaller concentration, even after annealing.

E. Comparison of NMR and macroscopic susceptibility in YBNO:Zn and YBNO:Cu: The low-T regime

A plot of $1/\chi_{SQUID}$ versus temperature done in the insets of Fig. 2 demonstrates that low-temperature susceptibility is
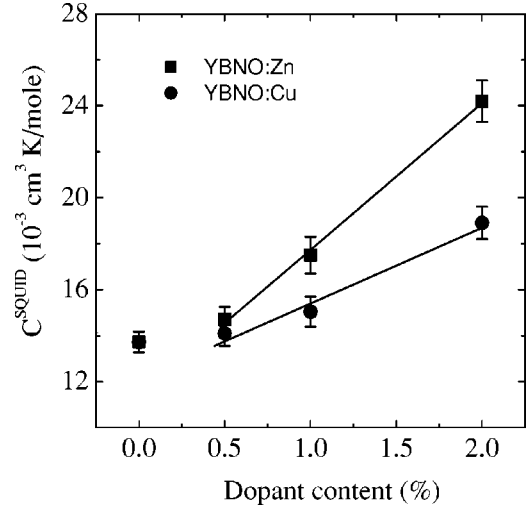
FIG. 18. Variation of the Curie constant C^{SQUID} extracted from the low-T susceptibility measurements vs impurity concentration for YBNO:Zn and YBNO:Cu. The linear fits (solid lines) were done without taking into account the Curie term of the "pure" sample, as the use of substituent might reduce the concentration of native defects in the latter.

dominated by a Curie term, which increases in the substituted compounds. In Fig. 18, we report the corresponding Curie constant C^{SQUID} with increasing impurity content for Cu and Zn. This proves that the substitution induces a paramagnetic contribution, as already has been shown by NMR at higher temperatures. This contribution seems to persist at temperatures as low as $T=2$ K. However, the pure Curie term appears similar in magnitude to the Zn or Cu contributions for concentrations of about 0.5%. A linear behavior of C^{SQUID} with increasing Zn or Cu concentration is expected. However, we found that the variation of C^{SQUID} with substituent concentration is nonlinear and is steeper for higher concentrations. This limits any straightforward quantitative interpretation of the data. This limitation is mainly due to the fact that in substituted samples, a sizable part of C^{SQUID} originates from defects other than the substitution itself (i.e., background Curie term as discussed in Sec. IV D). The precise variation of this background Curie term with the substituent concentration is unknown. It appears that impurity substitution (in small amounts) at Ni site helps to decrease this background Curie term as C^{SQUID} for Y$_2$BaNi$_{0.995}$Cu$_{0.005}$O$_5$ is almost identical to that of the pure whereas NMR showed that Cu induces a paramagnetic contribution. A rough estimate of the impurity contribution can still be made using the increase of C^{SQUID} for high enough dopant content. A linear fit (shown by solid lines in Fig. 18) without taking into account the pure composition leads to $C^{SQUID}_{Zn}=(6.4\pm0.7)\times10^{-3}$ cm^3 K/mole/% Zn and C^{SQUID}_{Cu} $=(3.3\pm0.6)\times10^{-3}$ cm^3 K/mole/% Cu.

In the Zn case, the NMR measurements allowed us to extract $C^{NMR}_{Zn}=(5.6\pm0.6)\times10^{-3}$ cm^3 K/mole/% Zn. There is a good agreement between macroscopic and local measurements even though they apply in different temperature ranges ($T\leqslant30$ K and 80 K$\leqslant T\leqslant$350 K, respectively). This value is not that far from the VBS simplified picture where

$C_{VBS} = 7.5 \times 10^{-3}$ cm^3 K/mole[6] originates from the two chain end $S = 1/2$ spins released by the introduction of Zn.

In the Cu case, if the doped $S = 1/2$ Cu acts as a free spin, its susceptibility should add to that of the induced staggered magnetization measured by NMR, leading to $\chi_{Cu}^{SQUID} = \chi_{Cu} + \chi_{Cu}^{NMR}(T)$. Anyhow, we found χ_{Cu}^{SQUID} to be smaller than $\chi_{Cu}^{NMR} = [(4.7 \pm 0.5)/T] \times 10^{-3}$ cm^3/mole/% Cu. This indicates that the introduced $S = 1/2$ does not act as a free spin, but magnetizes in the antiparallel orientation to the induced chain-end moments, at least at low T. This result is indeed expected if the Cu interacts antiferromagnetically with the nn chain-end Ni spins, in which case $\chi_{Cu} < 0$ is expected for $T < J'$. Such conclusion confirms then the comparison done previously between QMC simulations and our NMR results, which also leads to an antiferromagnetic coupling between Ni and Cu, with $J' \approx 40$ K.

V. CONCLUSION

We have probed impurity-induced magnetic effects in the Haldane chain compound YBNO via spinless (Zn) and $S = 1/2$ (Cu) substitutions at the Ni site. The Haldane gap remains unchanged upon substitution. The intensity analysis of the NMR satellites proves that the amount of dopant impurity present in the sample agrees well with the nominally intended stoichiometry. ^{89}Y NMR measurements show that Zn or Cu induce a staggered magnetization in their vicinity. Its magnitude decays exponentially with a characteristic length equal to the correlation length ξ of the infinite chain. The fit of the NMR shift data on a large-T range for the pure system with the results of QMC computations allows us to deduce a reliable value $J = 250 \pm 10$ K. For the Zn impurity the spatial dependence and magnitude of the staggered susceptibility observed by NMR matches perfectly the QMC calculated values with $J = 270 \pm 10$ K. For 70 K $< T < 350$ K, the total impurity-induced Curie susceptibility in the chain corresponds to an effective spin $S = 0.4 \pm 0.06$ on either side of the impurity for the Zn doped case, which is close to the theoretically predicted $S = 1/2$ excitation at $T = 0$.

In this high-T range, the induced staggered magnetization is slightly smaller for Cu which can be explained if the $S = 1/2$ Cu spin is coupled antiferromagnetically with the nearest neighbor Ni. A fit with the QMC calculated spin polarization allows us to deduce the magnitude $J' = (0.15 \pm 0.05)J$ of this AF coupling. This occurrence of an AF coupling between the Cu and the Ni is confirmed by the fact that the macroscopic susceptibility induced by Cu as measured by SQUID is even smaller for Cu impurities than for Zn impurities for $T < 30$ K. This confirms that in this T range the Cu magnetization opposes that of the local moments of the chain ends, as can be expected for an AF J'.

Further experiments are needed to follow the low-T behavior of the local magnetization both for Zn and Cu. In the case of Zn this would allow to check whether a Curie law applies to the lowest temperatures, below $T \approx \Delta$, as questioned by recent macroscopic measurements which find a sub-Curie behavior,[16] something not well-understood theoretically. As for the Cu case this would allow us to better follow the modifications of local magnetization for $T \approx J'$ as strong deviations from that observed for spinless impurities are expected. In case of high-T_c cuprates (e.g., YBa$_2$Cu$_3$O$_7$), substitution of Cu by magnetic (Ni) or nonmagnetic (Zn) impurity,[4] generates an induced polarization, with same temperature dependence of the staggered magnetization in both cases, but with weaker effects for Ni than Zn. This is qualitatively similar to the present study on a much simpler 1D chain. Such results confirm that magnetic or nonmagnetic substitutions also provide a good approach to probe the magnetic correlations of pure 2D systems.

[1] M. Takigawa, N. Motoyama, H. Eisaki, and S. Uchida, Phys. Rev. B **55**, 14 129 (1997).

[2] J.F. DiTusa, S-W. Cheong, J.-H. Park, G. Aeppli, C. Broholm, and C.T. Chen, Phys. Rev. Lett. **73**, 1857 (1994).

[3] N. Fujiwara, H. Yasuoka, Y. Fujishiro, M. Azuma, and M. Takano, Phys. Rev. Lett. **80**, 604 (1998).

[4] A.V. Mahajan, H. Alloul, G. Collin, and J.F. Marucco, Phys. Rev. Lett. **72**, 3100 (1994); J. Bobroff, H. Alloul, Y. Yoshinari, A. Keren, P. Mendels, N. Blanchard, G. Collin, and J.F. Marucco, *ibid.* **79**, 2117 (1997); J. Bobroff, W.A. MacFarlane, H. Alloul, P. Mendels, N. Blanchard, G. Collin, and J.F. Marucco, *ibid.* **83**, 4381 (1999); S. Ouazi, J. Bobroff, H. Alloul, and W.A. MacFarlane, cond-mat/0307728 (unpublished).

[5] F.D.M. Haldane, Phys. Lett. **93A**, 464 (1983); Phys. Rev. Lett. **50**, 1153 (1983).

[6] I. Affleck, T. Kennedy, E.H. Lieb, and H. Tasaki, Phys. Rev. Lett. **59**, 799 (1987).

[7] T. Kennedy, J. Phys.: Condens. Matter **2**, 5737 (1990).

[8] D.J. Buttrey, J.D. Sullivan, and A.L. Reingold, J. Solid State Chem. **88**, 291 (1990).

[9] J. Darriet and L.P. Regnault, Solid State Commun. **86**, 409 (1993).

[10] B. Batlogg, S-W. Cheong, and L.W. Rupp, Jr., Physica B **194-196**, 173 (1994).

[11] T. Yokoo, Y. Sakaguchi, K. Kakurai, and J. Akimitsu, J. Phys. Soc. Jpn. **64**, 3651 (1995).

[12] Y. Sakaguchi, K. Kakurai, T. Yokoo, and J. Akimitsu, J. Phys. Soc. Jpn. **65**, 3025 (1996).

[13] G. Xu, J.F. DiTusa, T. Ito, K. Oka, H. Takagi, C. Broholm, and G. Aeppli, Phys. Rev. B **54**, R6827 (1996).

[14] T. Shimizu, D.E. MacLaughlin, P.C. Hammel, J.D. Thompson, and S-W. Cheong, Phys. Rev. B **52**, R9835 (1995).

[15] A.P. Ramirez, S-W. Cheong, and M.L. Kaplan, Phys. Rev. Lett. **72**, 3108 (1994).

[16] C. Payen, E. Janod, K. Schoumacker, C.D. Batista, K. Hallberg, and A.A. Aligia, Phys. Rev. B **62**, 2998 (2000).

[17] F. Tedoldi, R. Santachiara, and M. Horvatić, Phys. Rev. Lett. **83**, 412 (1999).

[18] M. Kenzelmann, G. Xu, I.A. Zaliznyak, C. Broholm, J.F. DiTusa, G. Aeppli, T. Ito, K. Oka, and H. Takagi, Phys. Rev. Lett. **90**, 087202 (2003).

[19] C.D. Batista, K. Hallberg, and A.A. Aligia, Phys. Rev. B **58**, 9248 (1998).

[20] S. Botti, A. Rosso, R. Santachiara, and F. Tedoldi, Phys. Rev. B **63**, 012409 (2001).

[21] S. Miyashita and S. Yamamoto, Phys. Rev. B **48**, 913 (1993).

[22] F. Alet and E.S. Sørensen, Phys. Rev. B **62**, 14 116 (2000).

[23] E.S. Sørensen and I. Affleck, Phys. Rev. B **51**, 16 115 (1995).

[24] E. Polizzi, F. Mila, and E.S. Sørensen, Phys. Rev. B **58**, 2407 (1998).

[25] R.D. Shannon and C.T. Prewitt, Acta Crystallogr., Sect. B: Struct. Crystallogr. Cryst. Chem. **B25**, 925 (1969).

[26] A.W. Sandvik and J. Kurkijärvi, Phys. Rev. B **43**, 5950 (1991).

[27] A.W. Sandvik, J. Phys. A **25**, 3667 (1992).

[28] F. Alet, S. Wessel, and M. Troyer, cond-mat/0308495 (unpublished).

[29] O.F. Syljuäsen and A.W. Sandvik, Phys. Rev. E **66**, 046701 (2002).

[30] O.F. Syljuäsen, Phys. Rev. E **67**, 046701 (2003).

[31] F. Tedoldi, A. Rigamonti, C. Brugna, M. Corti, A. Lascialfari, D. Capsoni, and V. Massarotti, J. Appl. Phys. **83**, 6605 (1998).

[32] I. Affleck, Phys. Rev. B **41**, 6697 (1990); (private communication); [reported in M. Takigawa, T. Asano, Y. Ajiro, and M. Mekata, Phys. Rev. B **52**, R13 087 (1995)].

[33] T. Ami, M.K. Crawford, R.L. Harlow, Z.R. Wang, D.C. Johnston, Q. Huang, and R.W. Erwin, Phys. Rev. B **51**, 5994 (1995).

[34] Y.J. Kim, M. Greven, U.J. Wiese, and R.J. Birgeneau, Eur. Phys. J. B **4**, 291 (1998).

[35] Please note that the QMC results presented here and in Ref. 22 are totally compatible, even though the values of the hyperfine field obtained are not the same. The only things that differ in the two studies are the input parameters to fit the experiments. Indeed, the value of J used in both studies differ by 10%, and the Lande factor g was assumed to be around 2.4 in Ref. 22, while it was more reasonably assumed to be 2 in the current study.

[36] P. Roos and S. Miyashita, Phys. Rev. B **59**, 13 782 (1999).

[37] T. Tonegawa and M. Karubaki, J. Phys. Soc. Jpn. **64**, 3956 (1995).

[38] M. Troyer, B. Ammon, and E. Heeb, Lect. Notes Comput. Sci. **1505**, 191 (1998); the source code can be obtained from http://alps.comp-phys.org